Syntheses, structures and magnetic properties of manganese-lanthanide hexanuclear complexes

Takuya Shiga [a], Norihisa Hoshino [a], Hiroyuki Nojiri [b], and Hiroki Oshio [a,*]

[a] *Graduate School of Pure and Applied Sciences, University of Tsukuba, Tennodai 1-1-1, Tsukuba 305-8571, Japan*

[b] *Institute of Material Research, Tohoku University, Katahira 2-1-1, Aoba-ku, Sendai 980–8577, Japan*

We dedicate this article to Professor Dante Gatteschi for his contribution to molecular magnetism.

Abstract

Reactions of manganese acetate and lanthanide acetate with a Schiff-base ligand (H_3beemp = 2,6-bis[((2-(2-hydroxyethoxy)ethyl)imino)methyl]-4-methylphenol) yielded hexanuclear clusters of $[Mn^{III}_4Ln^{III}_2(\mu_3\text{-}O)_2(Hbeemp)_2(OAc)_8(\mu_3\text{-}OMe)_2(H_2O)_2]\cdot C_8H_{17}OH$ (Ln = Gd, Tb, and Y for **1**, **2**, and **3** respectively). Magnetic susceptibility measurements revealed that the mixed

spin systems of **1** and **2** showed ferrimagnetic behavior, while antiferromagnetic interactions were operative among Mn^{3+} ions in **3**. Ac magnetic susceptibility measurements for **2** showed frequency dependent in- and out-of-phase signals, confirming slow magnetic relaxation of spin reorientaions.

1. Introduction

Strong magnets such as Nd-Fe and Sm-Co alloys have large energy products ($(BH)_{max}$ values) due to large magnetic anisotropy of 4f metal elements,[1] and molecule based compounds with 3d and 4f metal ions have been attracted intense research interest to prepare bulk magnets, [2] single molecule magnets (SMMs)[3] and single chain magnets (SCMs).[4] Lanthanide ions with large magnetic anisotropy are suitable for SMM, however, magnetic interactions between paramagnetic lanthanide ions are very weak because of their shrunk f orbitals. It was, therefore, expected that mixed spin systems of 3d and 4f metal ion may have stronger magnetic interactions, and some SMMs of $[Cu_2Tb_2]$,[3a] $[Mn_6Dy_6]$, [3c] and $[Mn_2Dy_2]$ [3d] were prepared along this strategy. On the other hand, lanthanide ions have large ionic radii with coordination numbers larger than six, large coordination environment is necessary to assemble lanthanide

ions. We have prepared multinuclear 3d-metal complexes by using Schiff-base ligands with alkoxo groups.[5] We extended our research to prepare larger bridging Schiff-bases by introducing alkoxyether groups. We report here syntheses, structures, and magnetic properties of three mixed metal complexes of $[Mn_4Ln_2(\mu_4\text{-}O)_2(Hbeemp)_2(OAc)_4(OMe)_2(H_2O)_2]\cdot C_8H_{17}OH$ (H_3beemp = 2,6-bis[((2-(2-hydroxyethoxy)ethyl)imino)methyl]-4-methylphenol; Ln = Gd, Tb, and Y).

2. Experimental

2.1. Materials

All chemicals were purchased from commercial sources and used without further purification. 2,6-Diformyl-4-methylphenol was prepared according to the literature method.[6]

*2.2. Synthesis of $[Mn^{III}_4Gd^{III}_2(\mu_3\text{-}O)_2(Hbeemp)_2(OAc)_8(\mu_3\text{-}OMe)_2(H_2O)_2]\cdot C_8H_{17}OH$ (**1**·OctOH)*

To a solution of 2,6-diformyl-4-methylphenol (164 mg, 1.0 mmol), 2-(2-aminoethoxy)ethanol (210 mg, 2.0 mmol), and triethylamine (606 mg, 6.0 mmol) in methanol (10 ml) was added $Mn(OAc)_2\cdot 4H_2O$ (490 mg, 2.0 mmol) in methanol (10 ml), and the mixture was stirred for several minutes.

$Gd(OAc)_3{\cdot}4H_2O$ (408 mg, 1.0 mmol) in methanol (10 ml) was added to the resulting solution. The reaction mixture was refluxed for 20 min. After cooling to room temperature, the resulting solution was filtrated and *n*-octanol (40 ml) was added to the filtrate. The dark brown solution was diffused with diethyl ether to give brown platelets, $[Mn^{III}_4Gd^{III}_2(\mu_3\text{-}O)_2(Hbeemp)_2(OAc)_8(\mu_3\text{-}OMe)_2(H_2O)_2]{\cdot}C_8H_{17}OH$ (**1**·OctOH), suitable for single crystal X-ray structure analysis. They were collected by suction filtration and air-dried. Anal. Calcd. for $C_{60}H_{110}N_4Gd_2Mn_4O_{38}$: C, 35.50; H, 5.46; N, 2.76. Found: C, 35.22; H, 5.18; N, 2.76 %. IR (KBr disk): ν = 1647.1, 1624.0, 1591.2, 1413.7cm^{-1}.

2.3. Synthesis of $[Mn^{III}_4Tb^{III}_2(\mu_3\text{-}O)_2(Hbeemp)_2(OAc)_8(\mu_3\text{-}OMe)_2(H_2O)_2]{\cdot}C_8H_{17}OH$ *(**2**·OctOH)*

This complex was prepared by the same method as **1**, using $Tb(OAc)_3{\cdot}4H_2O$ instead of $Gd(OAc)_3{\cdot}4H_2O$. Anal. Calcd. for $C_{52}H_{88}N_4Mn_4O_{35}Tb_2$: C, 33.45; H, 4.75; N, 3.00. Found: C, 33.10; H, 4.67; N, 3.35 %. IR (KBr disk): ν = 1647.1, 1624.0, 1591.2, 1413.7 cm^{-1}.

2.4. Synthesis of $[Mn^{III}_4Y^{III}_2(\mu_3\text{-}O)_2(Hbeemp)_2(OAc)_8(\mu_3\text{-}OMe)_2(H_2O)_2]{\cdot}C_8H_{17}OH$ *(**3**·OctOH)*

This complex was prepared by the same method as **1**, using $Y(OAc)_3{\cdot}4H_2O$

instead of $Gd(OAc)_3{\cdot}4H_2O$. Anal. Calcd. for $C_{56}H_{95}N_4Mn_4O_{34.5}Y_2$: C, 37.92; H, 5.40; N, 3.16. Found: C, 37.70; H, 5.50; N, 2.90 %. IR (KBr disk): ν = 1645.2, 1622.0, 1593.1, 1417.6 cm^{-1}.

2.5. Physical measurements

Magnetic susceptibility data were collected in the temperature range of 1.8 K to 300 K in an applied field of 500 Oe by using a Quantum Design model MPMS-XL SQUID magnetometer. Pascal's constants were used to determine the diamagnetic corrections. Ac magnetic susceptibility measurements were carried out on a Quantum Design model PPMS with ACDC probe attachment in the frequency range of 1 kHz –10 kHz in the ac field of 3.0 Oe. HF-EPR spectra were measured by using a simple transmission method with three types of radiation sources: Gunn oscillators, backward wave oscillators, and a far-infrared laser. An InSb bolometer was used as a detector.

2.6. X-ray crystallography

Each brown columnar crystal of **1** (0.49 x 0.20 x 0.20 mm^3), **2** (0.29 x 0.10 x 0.07 mm^3), and **3** (0.31 x 0.11 x 0.10 mm^3) was mounted on the tip of a glass fiber with epoxy resin. Diffraction data were collected at 200 K on a Bruker SMART APEX diffractometer with a CCD type area detector, and a full sphere of data were collected using graphite-monochromated Mo–Kα radiation (λ =

0.71073 Å). At the end of data collection, the first 50 frames of data were recollected to establish that the crystal had not deteriorated during the data collection. The data frames were integrated using SAINT and were merged to give a unique data set for structure determination. Total reflections collected were 11379, 13067, and 11423 for **1**-**3**, respectively, of which independent reflections were 7875 (R(int) = 0.0454), 8872 (R(int) = 0.0531), and 7887 (R(int) = 0.0376). The structures were solved by direct methods and refined by the full-matrix least-squares method on all F^2 data using the SHELXTL 5.1 package (Bruker Analytical X-ray Systems). Hydrogen atoms were included in calculated positions and refined with isotropic thermal parameters riding on those of the parent atoms. Empirical absorption corrections were performed to yield minimum-max value of 0.3777–0.6382, 0.5141–0.8364, and 0.5392–0.8046, for **1**-**3**, respectively.

Crystallographic data for **1**-**3** have been deposited at the Cambridge Crystallographic Data Centre as the publication citation and deposition numbers CCDC 676579 – 676581. Copies of the data can be obtained free of charge on application to CCDC, 12 Union Road, Cambridge CB21EZ, UK, fax: (+44)1223-336-033; e-mail: deposit@ccdc.cam.ac.uk). A summary of the crystallographic parameters and data is given in Table 1.

[Insert Table 1]

3. Result and discussion

3.1. Crystal structures

Isomorphous crystals of **1** - **3** crystallized in the triclinic space group $P\bar{1}$ (Figure 1) and the selected bond lengths are tabulated in Table 2. Complex molecules in **1** - **3** lie on the inversion center. H_3beemp has five oxygen and two nitrogen donor atoms from one phenol, two imono, and two alkoxo groups, and mono anionic Hbeemp acts as a quinquedentate ligand, where one alkoxo group bridges Ln^{3+} and Mn^{3+} ions and the other alkoxo group remains uncoordinated. Each complex molecule has a hexanuclear core of two Ln^{3+} and four Mn^{3+} ions. In the hexanuclear core, butterfly shaped Ln_2Mn_2 cores (tetranuclear core) are supported by two μ_2-alkoxo, two μ_3-methoxo groups and two μ_3-oxide ions, and the remaining Mn^{3+} ions are linked through two acetate groups and phenol to the tetranuclear core. Mn1 and Mn2 ions have six coordination structures with N_1O_5 and O_6 chromophores from one bidentate Hbeemp, one unidentate μ_3-O^{2-} ion, and three unidentate acetate ions, and from one alkoxo group of ligand and two unidentate MeO^- ions and two unidentate acetate ions, respectively. Coordination bond lengths about Mn2 ions in **1** – **3** are 1.859(2) – 2.254(2) Å,

1.852(4) – 2.245(4) Å, and 1.861(3) – 2.232(2) Å, respectively, where the Jahn-Teller axes are along the O2-Mn2-O11 bonds. The Mn1 ions in **1** – **3** do not show distinct axial Jahn-Teller distortion with bond lengths of 1.822(2) – 2.086(2) Å, 1.818(4) – 2.092(4) Å, and 1.817(3) – 2.080(3) Å, respectively. The lanthanide ions have N_1O_8 coordination from one quadridentate Hbeemp, two unidentate acetate ions, one unidentate μ_3-O^{2-} ion and one water molecule. Ln^{3+}-O bond lengths are 2.342(2) – 2.596(2) Å, 2.295(4) – 2.576(4) Å, and 2.285(2) – 2.598(3) Å for Gd^{3+}, Tb^{3+}, and Y^{3+} ions, respectively.

[Insert Figure 1]

[Insert Table 2]

3.2. Magnetic properties

Magnetic susceptibility measurements were performed in the temperature range of 1.8 – 300 K and results are shown in $\chi_m T$ vs. T plots (Figure 2). A $\chi_m T$ value for **1** is 26.72 emu mol^{-1} K at 300 K, which is smaller than the value (27.75 emu mol^{-1} K) expected for the uncorrelated four Mn^{3+} ions (S = 2 with g = 2) and two Gd^{3+} ions ($^8S_{7/2}$, S = 7/2, L = 0, J = 7/2, g_J = 2), and this value remains constant down to 150 K. On further cooling of **1**, the $\chi_m T$ values decreased, reaching the minimum value of 20.647 emu mol^{-1} K at 4.0 K, followed by the slight increase. This temperature dependence suggests that **1**

has a high spin ground state due to ferrimagnetic interactions.

[Insert Figure 2]

The $\chi_m T$ value for **2** is 35.47 emu mol^{-1} K at 300 K and this is smaller than the value (35.63 emu mol^{-1} K) expected for uncorrelated four Mn^{3+} ions (S = 2, g = 2) and two Tb^{3+} ions ($^7F_6$; S = 2, L = 3, J = 6, g_J = 3/2). The temperature profile of $\chi_m T$ values of **2** is very similar to **1**, and $\chi_m T$ values reached the minimum value of 28.18 emu mol^{-1} K at 8.0 K, followed by the increase to 32.68 emu mol^{-1} K at 2.2 K. Compound **2** contains magnetically anisotropic Mn^{3+} and Tb^{3+} ions, hence, the analysis of the magnetic data is difficult due to significant orbital contribution from Tb^{3+} ions. Complex **2** is, on the other hand, expected to show slow magnetic relaxation of spin reorientation due to the magnetic anisotropy, which was confirmed by the observation of in- and out-of-phase signals in ac magnetic susceptibility measurements (Figure 3).

[Insert Figure 3]

3 has diamagnetic Y^{3+} ions, and the $\chi_m T$ value at 300 K is 11.13 emu mol^{-1} K, which is slightly smaller than the value (12.00 emu mol^{-1} K calculated for Mn^{3+} ions with S = 2 and g = 2) expected for uncorrelated four Mn^{3+} ions. $\chi_m T$ value decreases as the temperature was lowered, reaching the minimum value of 1.60 emu mol^{-1} K at 1.8 K, meaning antiferromagnetic interactions operative among

Mn^{3+} ions. Note that neither **1** nor **3** showed out-of-phase signals in the ac susceptibility measurements, suggesting that the slow magnetic relaxation in **2** is mainly due to magnetic anisotropy of Tb^{3+}.

4. High field epr (HF epr) spectra

HF epr spectra for powder samples of **1** - **3** were collected at several frequencies at 1.6 K. The spectra for **1** and **2** have two distinct peaks and one broad peak with a shoulder, respectively (Figures 4 and 5). Figure 6 shows plots of HF epr frequencies versus observed resonance magnetic fields for **1** and **2**. The resonance peaks observed in **1** and **2** were linearly shifted to the higher magnetic field region as the frequencies were increased. Resonance fields (B_r) for the transitions from an M_s to $M_s + 1$ state can be formulated as $B_r = h\nu/g\mu_B - (2M_s + 1)D$. Assuming the linear relation of ν and B_r values, the intercept values, which relate to the magnetic anisotropy, were 10 and 200 GHz for **1** and **2**, respectively. The amplitude of D values for **1** and **2** can not be obtained because the spin ground states have not been determined and the peak assignments remain unclear. However, the estimated intercept values suggest that the magnetic anisotropy of **2** is larger than that of **1**, and this is mainly due to the Tb^{3+} ions in **2**. Note that **3** did not show an epr signals, and this is in

consistent with the fact of its singlet ground state.

[Insert Figure 4]

[Insert Figure 5]

[Insert Figure 6]

5. Conclusion

A series of heterometal 3d-4f hexanuclear complexes, $[Mn^{III}_4Ln^{III}_2(\mu_3\text{-}O)_2(Hbeemp)_2(OAc)_2(\mu_3\text{-}OMe)_2(H_2O)_2]\cdot C_8H_{17}OH$ (Ln = Gd, Tb, and Y) were prepared. **1** and **2** show ferrimagnetic behaviors due to antiferromagnetic interactions between metal ions, while **3** has dominant antiferromagnetic interactions among Mn^{3+} ions. **2** shows frequency dependent out-of-phase ac signals, and this may suggest that **2** is an SMM.

Acknowledgement. This work was supported by the TARA projects in the University of Tsukuba and by a Grant-in-Aid for Scientific Research from the Ministry of Education, Culture, Sports, Science and Technology, Japan.

References

[1] (a) M. Sagawa, S. Fujimura, M. Togawa, M. Matsumura, J. Appl. Phys. 55 (1984) 2083; (b) J.M.D. Coey, H. Sun, J. Mag. Magn. Mater. 87 (1990) L251.

[2] (a) M. Sakamoto, K. Manseki, H. Ōkawa, Coord. Chem. Rev. 219-221 (2001) 379; (b) R.E.P. Winpenny, Chem. Soc. Rev. 27 (1998) 447; (c) C. Benelli, D. Gatteschi, Chem. Rev. 102 (2002) 2369; (d) S.G. Chore, D.W. Knoeppel, H. Deng, J. Liu, J.P. White III, S.-H. Chun, J. Alloys Compd. 249 (1997) 25; (e) C.E. Plečnik, S. Liu, S.G. Shore, Acc. Chem. Res. 36 (2003) 499; (f) J.-P Sutter, M.L. Kahn, in: J.S. Miller, M. Drillon (Eds.), Magnetism: Molecules to Materials V. (2005) 161; (g) S. Tanase, J. Reedijk, Coord. Chem. Rev. 250 (2006) 2501.

[3] (a) S. Osa, T. Kido, N. Matsumoto, N. Re, A. Pochaba, J. Mrozinski, J. Chem. Soc. Chem. 126 (2004) 420; (b) A. Mishra, W. Wernsdorfer, K.A. Abboud, G. Christou, J. Am. Chem. Soc. 126 (2004) 15648; (c) C.M. Zaleski, E.C. Depperman, J.W. Kampf, M.L. Kirk, V.L. Pecoraro, Angew. Chem. Int. Ed. 43 (2004) 3912; (d) A. Mishra, W. Wernsdorfer, S. Parsons, G. Christou, E.K. Brechin, Chem. Commun. (2005) 2086; (e) M. Ferbinteanu, T. Kajiwara, K.-Y Choi, H. Nojiri, A. Nakamoto, N. Kojima, F. Cimpoesu, Y. Fujimura, S. Takaishi, M. Yamashita, J. Am. Chem. Soc. 128 (2006) 9008; (f) C. Aronica, G. Pilet, G.

Chastanet, W. Wernsdorfer, J.-F. Jacquot, D. Luneau, Angew. Chem. Int. Ed. 45 (2006) 4659.

[4] (a) K. Bernot, L. Bogani, A. Caneschi, D. Gatteschi, R. Sessoli, J. Am. Chem. Soc. 128 (2006) 7947; (b) L. Bogani, C. Sangregorio, R. Sessoli, D. Gatteschi, Angew. Chem. Int. Ed. 44 (2005) 5817; (c) K. Bernot, L. Bogani, R. Sessoli, D. Gatteschi, Inorg. Chim. Acta 360 (2007) 3807.

[5] (a) S. Yamashita, T. Shiga, M. Kurashina, M. Nihei, H. Nojiri, H. Sawa, T. Kakiuchi, H. Oshio, Inorg. Chem. 46 (2007) 3810; (b) H. Oshio, M. Nihei, A. Yoshida, H. Nojiri, M. Nakano, A. Yamaguchi, Y. Karaki, H. Ishimoto, Chem. Eur. J. 11 (2005) 843; (c) H. Oshio, N. Hoshino, T. Ito, M. Nakano, J. Am. Chem. Soc. 126 (2004) 8805; (d) S. Koizumi, M. Nihei, T. Shiga, M. Nakano, H. Nojiri, R. Bircher, O. Waldmann, S.T. Ochsenbein, H.U. Güdel, F. Fernandez-Alonso, H. Oshio, Chem. Eur. J. 13 (2007) 8445; (e) T. Shiga, H. Oshio, Polyhedron 26 (2007) 1881.

[6] (a) D.A. Denton, H. Suschitzky, J. Chem. Soc. (1963) 4741; (b) L.F. Lindoy, G.V. Meehan, N. Svenstrup, Synthesis (1998) 1029.

Table 1. Crystallographic data for complexes **1**-**3**.

Compound	**1**	**2**	**3**
Formula	$C_{59}H_{78}N_4O_{33}Mn_4Gd_2$	$C_{59}H_{78}N_4O_{33}Mn_4Tb_2$	$C_{59}H_{78}N_4O_{33}Mn_4Y_2$
Formula weight	1905.51	1908.85	1768.83
Crystal color	brown	brown	brown
Crystal habit	columnar	columnar	columnar
Crystal size / mm^3	0.49 x 0.20 x 0.20	0.29 x 0.10 x 0.07	0.31 x 0.11 x 0.10
Crystal system	Triclinic	Triclinic	Triclinic
Space group	$P\bar{1}$	$P\bar{1}$	$P\bar{1}$
Unit cell dimensions			
a / Å	10.310(2)	10.248(2)	10.304(2)
b / Å	14.161(3)	14.023(3)	14.093(3)
c / Å	14.433(3)	14.348(3)	14.390(3)
α / ^{o}	86.300(4)	85.732(4)	86.208(4)
β / ^{o}	70.840(4)	70.858(4)	71.027(4)
γ / ^{o}	71.591(4)	71.172(4)	71.467(4)
V / $Å^3$	1886.8(7)	1842.5(6)	1872.1(7)
Z	1	1	1
D_{calc} / Mg m^{-3}	1.677	1.720	1.569
Absorption coefficient / mm^{-1}	2.468	2.646	2.273
θ range / ^{o}	1.50 to 27.99	1.50 to 28.37	1.50 to 28.06
Reflections collected	11379	13067	11423
Independent reflections (R_{int})	7875 (0.0454)	8872 (0.0531)	7887 (0.0376)
Final R indices [$I > 2\sigma(I)$]	$R1$ = 0.0313	$R1$ = 0.0505	$R1$ = 0.0437
	$wR2$ = 0.0901	$wR2$ = 0.1238	$wR2$ = 0.1155
R indices (all data)	$R1$ = 0.0330	$R1$ = 0.0684	$R1$ = 0.0623
	$wR2$ = 0.0913	$wR2$ = 0.01314	$wR2$ = 0.1210
Goodness-of fit on F^2	1.071	0.938	0.997

Table 2. Selected interatomic distances (Å) for complexes **1**-**3**.

	1	**2**	**3**
Mn(1)-O(1)	1.822(2)	1.818(4)	1.817(3)
Mn(1)-N(2)	2.040(3)	2.033(5)	2.035(3)
Mn(1)-O(9)	2.041(2)	2.059(4)	2.053(3)
Mn(1)-O(12)	2.067(2)	2.092(4)	2.080(3)
Mn(1)-O(3)	2.079(2)	2.054(4)	2.064(3)
Mn(1)-O(10)	2.086(2)	2.050(4)	2.071(3)
Mn(2)-O(1)	1.859(2)	1.852(4)	1.861(3)
Mn(2)-O(5)$^{\#1}$	1.914(2)	1.908(4)	1.917(3)
Mn(2)-O(13)	1.961(2)	1.958(4)	1.959(3)
Mn(2)-O(2)$^{\#1}$	1.970(2)	1.959(4)	1.962(3)
Mn(2)-O(11)	2.210(2)	2.197(4)	2.212(3)
Mn(2)-O(2)	2.254(2)	2.245(4)	2.232(2)
Ln(1)-O(1)	2.324(2)	2.295(4)	2.285(2)
Ln(1)-O(14)	2.356(2)	2.366(4)	2.310(3)
Ln(1)-O(5)	2.368(2)	2.345(4)	2.331(3)
Ln(1)-O(8)	2.435(2)	2.392(4)	2.384(3)
Ln(1)-O(16)	2.497(2)	2.473(5)	2.444(3)
Ln(1)-O(3)	2.524(2)	2.506(4)	2.503(3)
Ln(1)-N(1)	2.542(3)	2.528(5)	2.513(3)
Ln(1)-O(4)	2.544(2)	2.523(4)	2.524(3)
Ln(1)-O(2)	2.596(2)	2.576(4)	2.598(3)

Key to symmetry operation: $^{\#1}$ –x+2, –y+1, –z+2

Figure captions

Figure 1. An ORTEP drawing of **1** – **3**, where the same numberings are used for **1** – **3**.

Figure 2. Plots of $\chi_m T$ vs. T for **1**(○), **2**(□), and **3**(Δ).

Figure 3. Plots of χ_m' vs. T and χ_m'' vs. T for **2**.

Figure 4. HF-EPR spectra of a microcrystalline sample for **1**.

Figure 5. HF-EPR spectra of a microcrystalline sample for **2**.

Figure 6. Plots of the field frequency versus resonance magnetic field for the observed peaks in **1** and **2**.

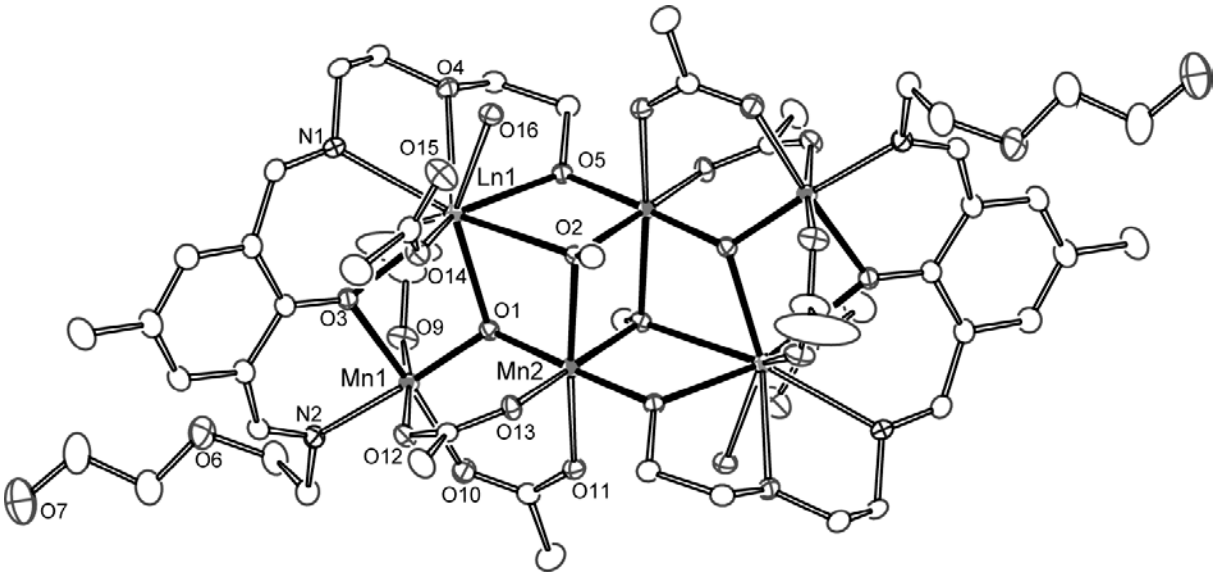
O4
N1
O15
O16
Ln1
O5
O2
O14
O3
O9
O1
Mn1
Mn2
N2
O13
O6
O12
O10
O11
O7

Figure 1.

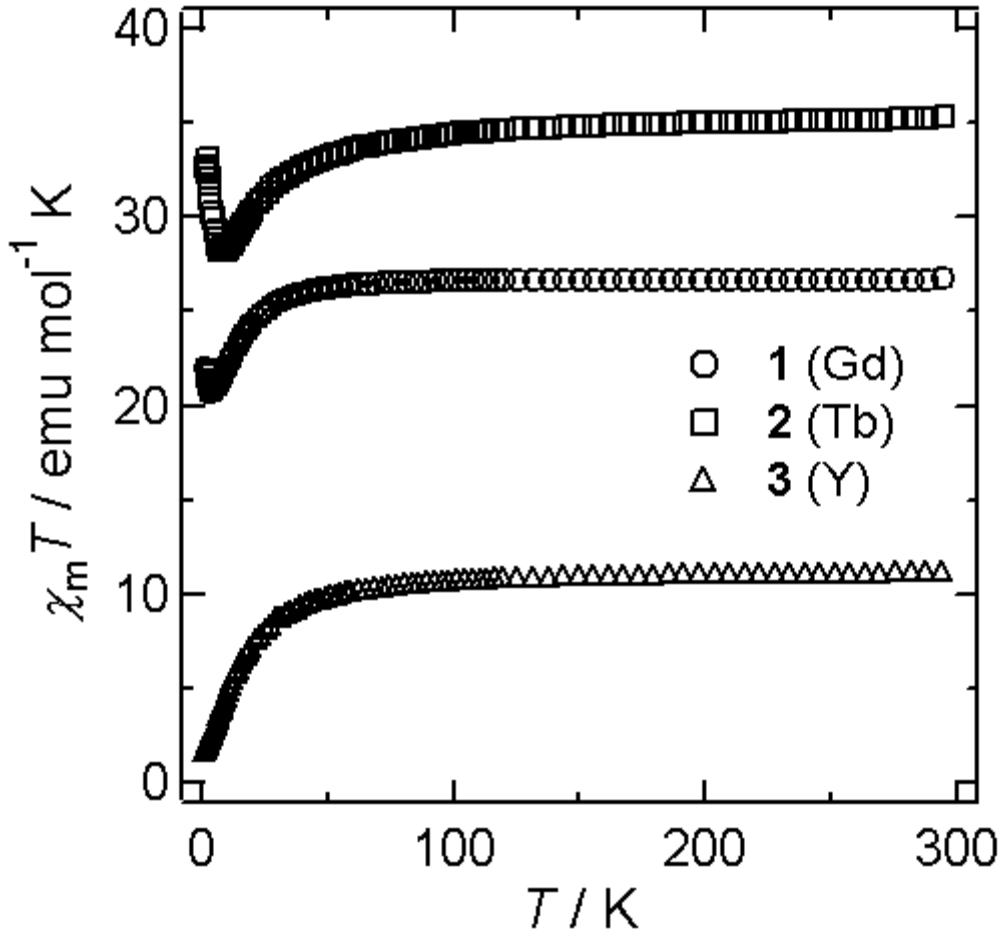

Figure 2.

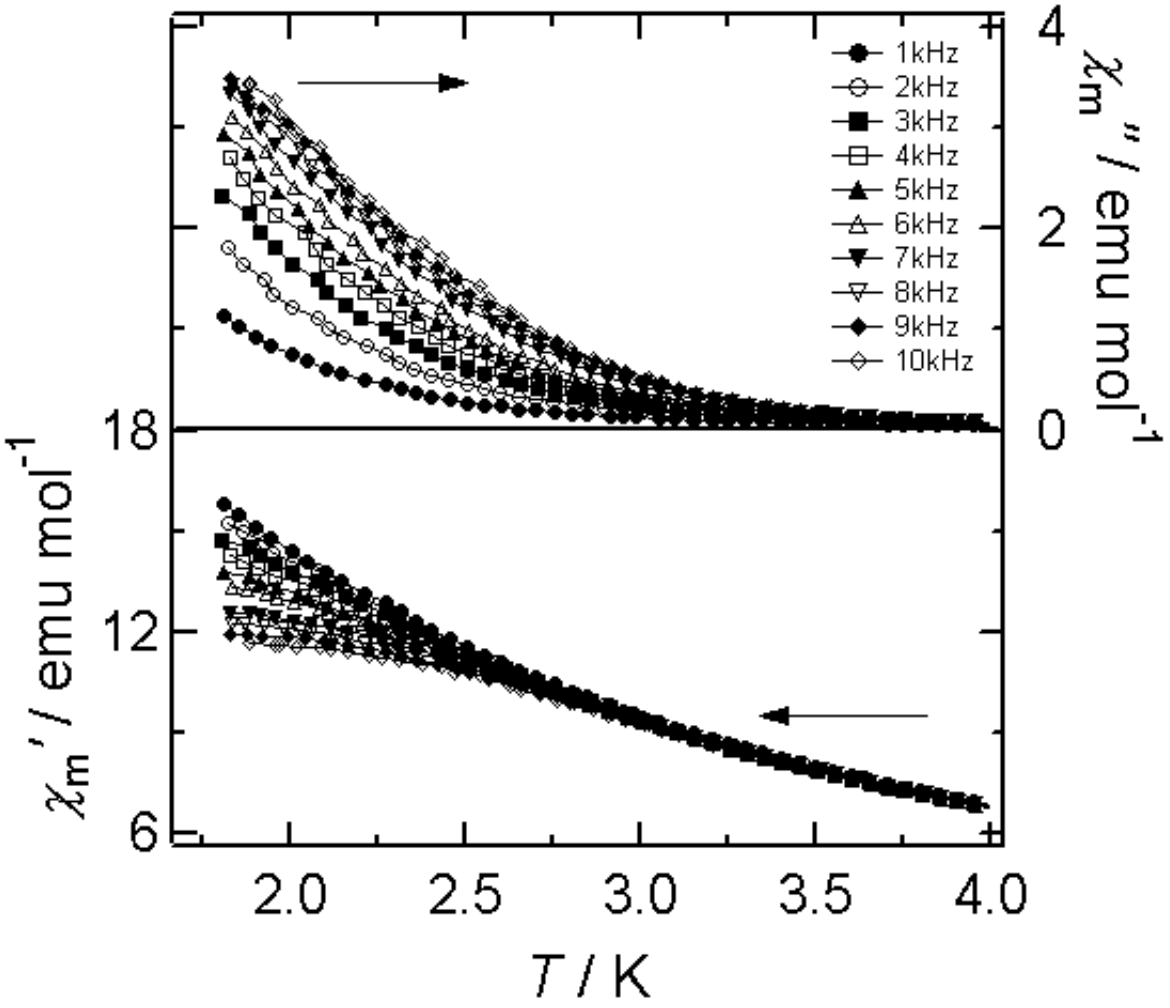
1kHz
2kHz
3kHz
4kHz
5kHz
6kHz
7kHz
8kHz
9kHz
10kHz
18
12
6
4
2
0
2.0
2.5
3.0
3.5
4.0
T / K
χm' / emu mol-1
χm'' / emu mol-1

Figure 3.

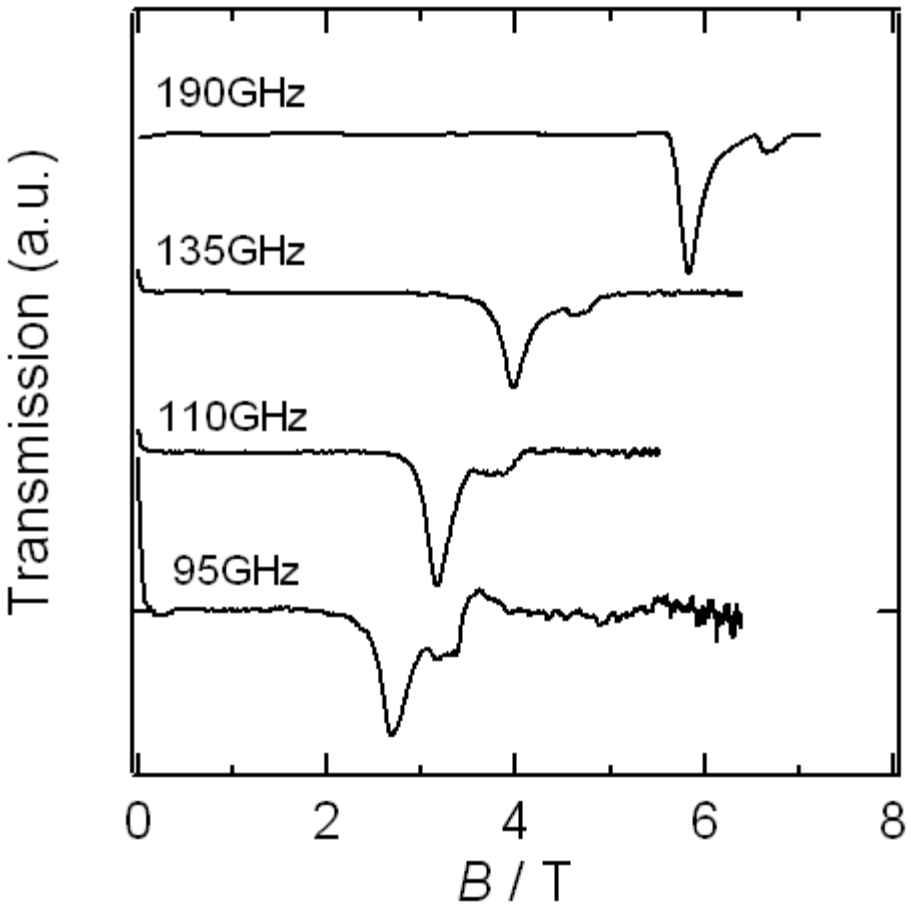

Figure 4.

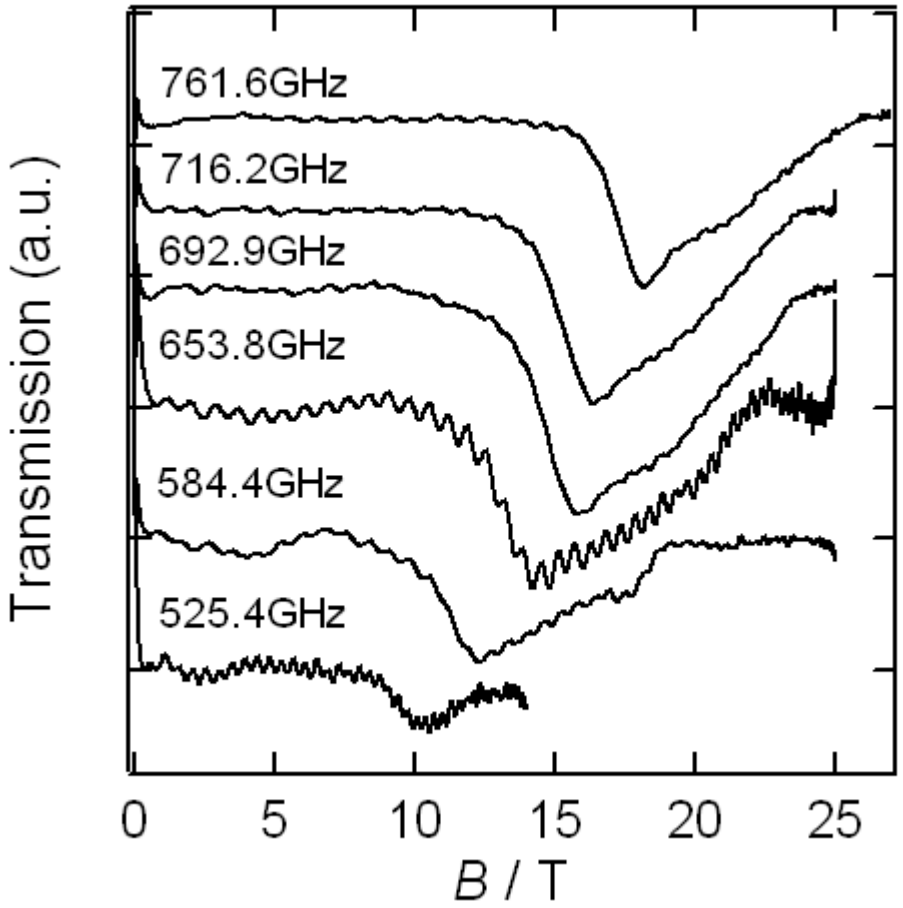
761.6GHz
716.2GHz
692.9GHz
653.8GHz
584.4GHz
525.4GHz
Transmission (a.u.)
0
5
10
15
20
25
B / T

Figure 5.

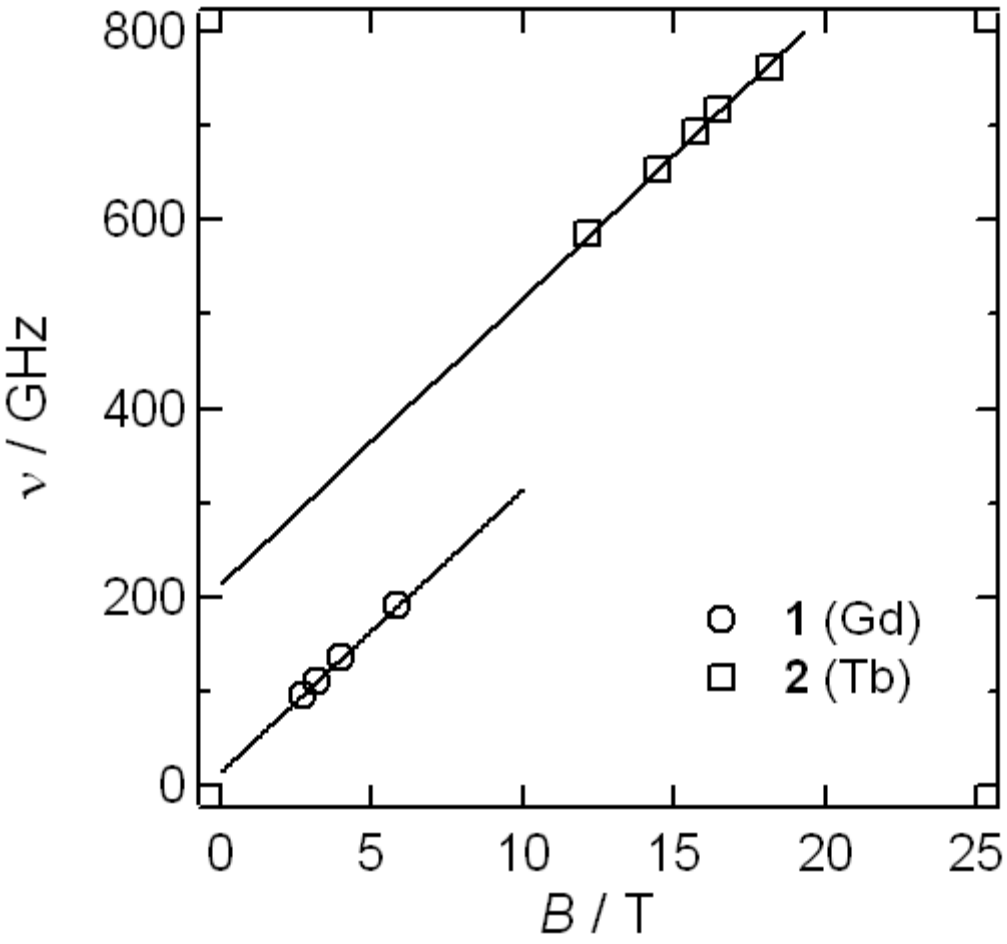

Figure 6.

Contents

Hexanuclear 3d-4f complexes of $[Mn^{III}_4Ln^{III}_2(\mu_3\text{-}O)_2(Hbeemp)_2(OAc)_8(\mu_3\text{-}OMe)_2(H_2O)_2]\cdot C_8H_{17}OH$ (H_3beemp = 2,6-bis[((2-(2-hydroxyethoxy)ethyl)imino)methyl]-4-methylphenol and Ln = Gd, Tb, and Y for **1**, **2**, and **3**, respectively.) were prepared. **1** and **2** show ferrimagnetic behaviors, while **3** has a singlet ground state due to antiferromagnetic interactions. Ac magnetic susceptibility measurements for **2** showed frequency dependent in- and out-of-phase signals, confirming slow magnetic relaxation.